Chemistry & Biology
Article

Small-Molecule Ligands of GD2 Ganglioside, Designed from NMR Studies, Exhibit Induced-Fit Binding and Bioactivity

Wenyong Tong,[1,2] Martin Gagnon,[1,2,11] Tara Sprules,[5] Michel Gilbert,[6] Shafinaz Chowdhury,[1] Karen Meerovitch,[3,7] Karl Hansford,[7] Enrico O. Purisima,[8] John W. Blankenship,[10,12] Nai-Kong V. Cheung,[9] Kalle Gehring,[3,5] William D. Lubell,[10] and H. Uri Saragovi[1,2,4,*]

[1]Lady Davis Institute-Jewish General Hospital, Montréal, QC, Canada, H3T 1E2
[2]Department of Pharmacology and Therapeutics
[3]Department of Biochemistry
[4]Department of Oncology and the Cancer Center
McGill University, Montréal, QC, Canada H3G 1Y6
[5]Quebec/Eastern Canada High Field NMR Facility, McGill University, Montréal, QC, Canada H3A 2A7
[6]Institute for Biological Sciences, National Research Council Canada, Ottawa, ON, Canada K1A 0R6
[7]Mimetogen Pharmaceuticals, Montreal, QC, Canada H3T 1E2
[8]Biotechnology Research Institute, National Research Council Canada, Montreal, QC, Canada H4P 2R2
[9]Department of Pediatrics, Memorial Sloan Kettering Cancer Center, New York, NY 10065, USA
[10]Department of Chemistry, Université de Montréal, Montréal, QC, Canada H3T 1N8
[11]Present address: Chlorion Pharmaceuticals, Montréal, QC, Canada
[12]Present address: Trubion Pharmaceuticals, Seattle, WA, USA
*Correspondence: uri.saragovi@mcgill.ca
DOI 10.1016/j.chembiol.2010.01.012

SUMMARY

Ganglioside GD2 is a cell surface glycosphingolipid. Targeting of GD2, i.e., by anti-GD2 mAb 3F8, is used clinically for cancer diagnosis, prognosis, and therapy. Here, the conformations of free GD2, and of GD2 bound to mAb 3F8, were resolved by saturation transfer difference NMR and molecular modeling. Then, three small-molecule cyclic peptide ligands that bind to GD2 selectively were designed. Transferred nuclear Overhauser enhancement of the GD2-bound conformation of the peptide ligands showed an induced-fit binding mechanism. The mAb 3F8 and the peptidic GD2 ligands mediate similar biological functions in cell-based assays of calcium fluxes and src activation. Thus, small molecules can selectively and functionally interact with a sugar head group. This work furthers the concept of rationally designing ligands for carbohydrate targets, and may be expanded to other clinically relevant gangliosides.

INTRODUCTION

The structures of the glycans protruding from eukaryotic plasma membranes change with the onset of cancer (Dube and Bertozzi, 2005) and other pathologies. For example, ganglioside GD2 is expressed during embryonic development, and in the adult it is normally expressed at very low levels in the peripheral nervous system and the cerebellum (Svennerholm et al., 1994; Yuki et al., 1997) but it is overexpressed in neuroblastomas, small-cell lung carcinomas, and melanomas (Cahan et al., 1982; Watanabe et al., 1982; Cheresh et al., 1986; Thurin et al., 1986). GD2 is thus targeted clinically for diagnosis and immunotherapy (Modak and Cheung, 2007) using anti-GD2 monoclonal antibodies (mAb), such as IgG3 mAb 3F8. The importance of gangliosides in tumorigenesis, tumor progression, and tumor metastasis may be due to their biological functions (Hakomori and Zhang, 1997; Birkle et al., 2003), which include cell recognition, cell matrix attachment, cell growth, or differentiation, including the induction of Ca^{2+} fluxes and the activation of the src family kinases (Gouy et al., 1994; Golard, 1998; Birkle et al., 2003).

Previously, the interactions of mAbs directed against ganglioside GT1a and GD3 were studied by saturation transfer difference (STD) nuclear magnetic resonance (NMR) spectroscopy and surface plasmon resonance (SPR) measurements (Houliston et al., 2007). Also, binding epitopes and conformations were obtained by STD and 2D NMR in the presence of GM1 micelles for natural peptides that interact with ganglioside GM1 (enkephalin [Chatterjee et al., 2004], amyloid peptide [Mandal and Pettegrew, 2004], and bradykinin [Chatterjee and Mukhopadhyay, 2005]). However, GD2 has not been studied in this manner; and more importantly generally the structural data obtained for carbohydrates have been impervious to the design of selective ligands with biological activity.

Here we studied whether NMR-based approaches can generate GD2-selective ligands with biological activity. We report the use of STD NMR spectroscopy (Meyer and Peters, 2003) to study the binding characteristics of anti-GD2 mAb 3F8 to two forms of GD2: (i) intact ganglioside GD2 in dodecylphosphocholine (DPC, that form micelles as a plasma membrane mimic), and (ii) the "GD2 carbohydrate head" as a water-soluble phenylthioether analog of GD2 that lacks ceramide and lipids.

Then we synthesized three GD2-selective peptidic ligands that mimic mAb 3F8 using mAb mimicry design (Saragovi et al., 1992). Their structures and their binding to GD2 micelles mimicking lipid rafts were studied by NMR. The conformation of the peptidic GD2 ligands bound to the head group of GD2 was characterized by transferred nuclear Overhauser enhancement (trNOE) experiments that demonstrated their conformational change on ganglioside binding, and a likely induced-fit mechanism. The peptides have biological activity similar to the original ligand mAb 3F8, in cell-based assays of calcium fluxes and src activation. This report demonstrates that a small-molecule peptide, designed from experimental binding data, can be a ligand that selectively and functionally interacts with a ganglioside sugar head group.

RESULTS AND DISCUSSION

Generation of a Soluble GD2 Analog for Structural Studies

Ganglioside GD2/3F8 interactions can be inhibited by soluble thiophenyl GD2 (Figure 1A) in a dose-dependent manner (Figure 1B). The IC_{50} of this water-soluble thiophenyl GD2 is ~10 μM. Competition is considered to be specific because thiophenyl GD3 does not affect the binding of ganglioside GD2 to 3F8. Thus, soluble thiophenyl GD2 can be considered a structural analog of ganglioside GD2.

Resonance Assignments of Ganglioside GD2 in DPC, Thiophenyl GD2 and Structure Calculations

The complete proton and carbon chemical shift assignments for ganglioside GD2 in DPC micelles and thiophenyl GD2 in aqueous solution are provided in Tables S1 and S2, respectively (available online). Fifty-one distance restraints, including one between glucose and the lipid tail ceramide, were obtained from 2D-ROESY for ganglioside GD2 in DPC micelles. The 2D-NOESY spectrum that was obtained on thiophenyl GD2 with a mixing time of 200 ms detected 48 NOEs, which were used to construct conformations of thiophenyl GD2 (Figure 2). The root-mean-square deviation (rmsd) within each group of conformers was ~0.7 Å excluding the 2 terminal residues. The structure of thiophenyl GD2 in water differed from that of ganglioside GD2 in DPC micelles (rmsd = 3.0 Å) primarily in the glycosidic dihedral angles $\varphi_4\phi_4\omega_4\chi_4$ (Figure 1A; Table S3), which means the terminal neuraminic acid residue can dynamically adopt different conformations in different chemical environments. The average value of $\varphi_2\phi_2$ is very similar to those reported by a molecular dynamics study, indicating that the conformation of the linkage between galactose and glucose is not influenced by the presence of other residues in the ganglioside (Vasudevan and Balaji, 2002). These structures demonstrated that the ceramide moiety interacted with the carbohydrate in a way that altered its conformation, which indicates that the conformations of head group and ceramide with lipid tail are interrelated and influenced by the micelle membrane (Vasudevan and Balaji, 2001).

The NMR conformers show a well-structured carbohydrate, which in a 10 ns MD simulation study was stable (data not shown). Next we studied how this stable structure behaves in the presence of ligands, such as mAb 3F8.

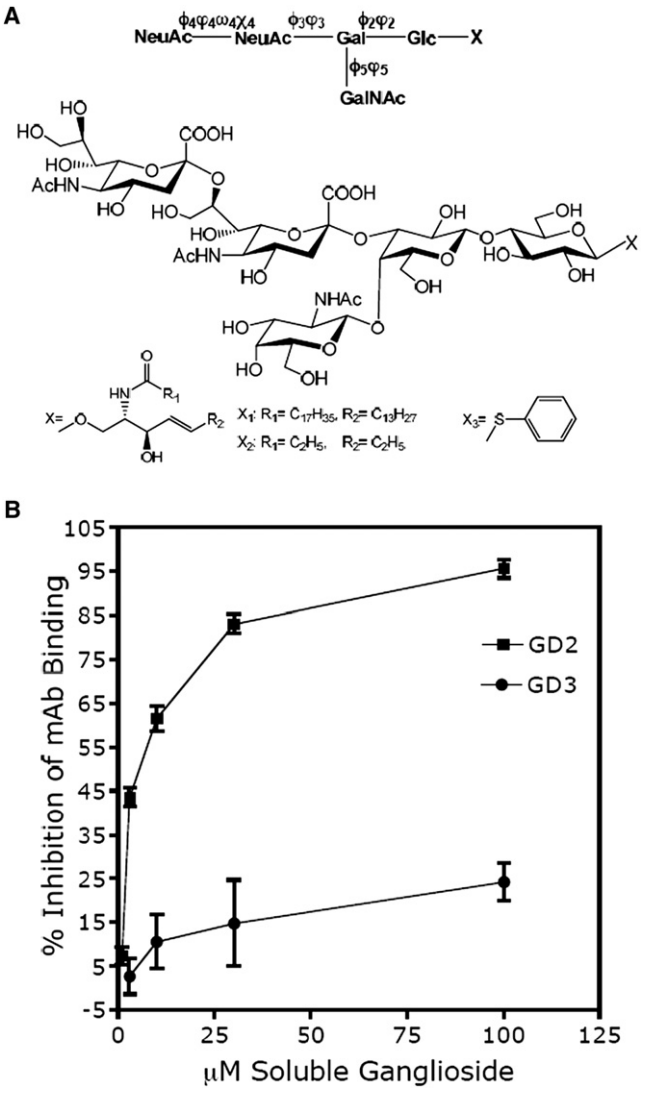

Figure 1. Structures and Antibody Binding of Ganglioside GD2 and its Derivatives

(A) The carbohydrate "head" of GD2 is shown, to which can be attached either a ceramide or lipid tail (X1), this is herein referred to as ganglioside GD2. The ceramide tail of ganglioside GD2 can be truncated (X2) for the purpose of modeling. X3 is a synthetic water-soluble thiophenyl GD2, lacking the ceramide and lipid tail, as an analog of ganglioside GD2. Residues and torsion angels are shown (also see Table S3).

(B) Soluble thiophenyl GD2 binds to anti-GD2 mAb 3F8 and therefore competes 3F8 binding to immobilized ganglioside GD2 in competitive ELISA. Soluble thiophenyl GD2 inhibited the binding of mAb 3F8 (5 ng/well) to immobilized GD2 (10 ng/well) in a dose-dependent manner with an IC_{50} of 10 μM. Shown is the average and standard error of the mean (SEM) from three independent assays. As control, soluble thiophenyl GD3 did not inhibit 3F8-ganglioside GD2 interactions; but did inhibit the binding of anti-GD3 mAb R24 to ganglioside GD3 (data not shown).

Group Epitope Mapping (GEM): The Binding Interactions of Thiophenyl GD2 and Ganglioside GD2 with mAb 3F8

STD signals show that the binding of soluble thiophenyl-GD2 to 3F8 can be resolved (Figures 3A and 3B; Figure S2). The most prominent peaks in the STD spectra arise from the resonances

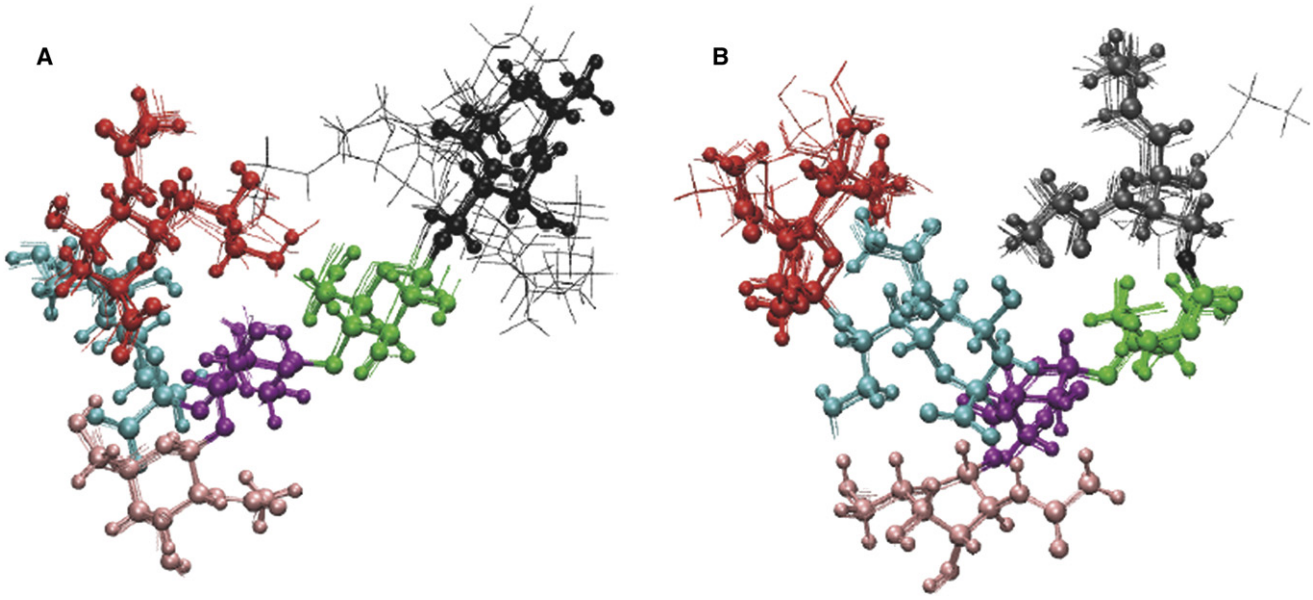

Figure 2. Superimposition of GD2 Structures as Determined from Annealing Simulation with Refinement of NMR

(A) Ensemble of thiophenyl GD2 structures (14 conformers).

(B) Ensemble of GD2 ganglioside structures with truncated lipid tails (16 conformers). Glucose = green, galactose = purple, N-acetyl galactosamine = pink. Two N-acetyl neuraminic acids are in blue (NeuAc (2-3)) and red NeuAc (2-8). For modeling, both ceramide and thiophenyl groups were replaced by a truncated ceramide (black) with a shorter sphingosine and fatty acid. The reference structure is in CPK representation, and the others are in line representation.

of the neuraminic acids (NeuAc) (2-3) residue connected to galactose (Gal). The H3 equatorial (eq) proton of NeuAc (2-3) experiences the largest STD amplification factor (Figure 3C). Integral values from the reference and STD spectrum show that if the largest signal, H3eq, is set to 100% (T_{sat} = 5 s), the H2 proton of β-glucose (Glc) and the N-acetyl methyl resonances reach about 38% and 25%, respectively (Figure 3D). Small contributions are also observed for protons at 3.8–3.9 ppm and 3.6–3.7 ppm, which could arise from β-glucose, NeuAc (2-3), and NeuAc (2-8). However, the signal is not strong enough to distinguish individual contributions. For the anomeric protons of glucose and N-acetyl galactosamine (GalNAc), no obvious STD response was observed, which may be due to their close proximity to the HDO resonance.

The intensities of the observed STDs are primarily dependent upon the longitudinal relaxation rate of the free ligand proton at long saturation times (Yan et al., 2003). This is seen at the long saturation times (1–5 s) employed in our experiments (Table S4). The methyl groups and Glc/Gal H2 protons have the longest T1s, and in the STD spectra give more significant signals than other sugar protons falling between 3.6 and 3.9 ppm.

The proton of NeuAc (2-3) H3 eq, which has a short T1 (0.7 s), showed the largest amplification factor at different saturation times (data not shown). This indicates that the side of sugar rings with the N-acetyl group and carboxylic acid is directed toward the antibody. Additional STD experiments with increasing concentrations of thiophenyl-GD2 shows that a maximum amplification is reached for the more weakly interacting protons at 1 mM (Figure 3C). The more strongly interacting proton did not reach maximum amplification under the experimental conditions. Any possible nonspecific contribution to this binding cannot be excluded at this time (Ji et al., 2009), because there is no high-affinity inhibitor to saturate the specific binding site.

The STD NMR profile of ganglioside GD2 embedded in DPC micelles showed that the water-exposed sugar head groups could also interact with the antibody. The STD spectrum of GD2 ganglioside in DPC micelles interacting with mAb 3F8 showed that additional peaks of sugar and ceramide are observed at 3.8–3.9 ppm, the peaks from the acetyl methyl resonances are enhanced, and a new DPC peak at 3.28 ppm appears (Figure S2).

The control STD spectrum of GD2 ganglioside in DPC micelles with no mAb 3F8 shows signals arising from the methyl groups of neuraminic acid and N-acetyl galactose, and from DPC, caused by irradiation of the DPC micelle or by nonspecific interaction of these methyl groups with the DPC micelle.

To confirm whether signals in the STD spectrum in the presence of mAb 3F8 arise from saturation transfer from the mAb, the on-resonance saturation frequency was shifted from −2 to 9 ppm. This resulted in a very similar STD spectrum, indicating that the GD2 head group did interact with mAb 3F8 in this membrane-like environment. The low signal to noise in the STD spectra of the GD2/mAb spectra made it difficult to obtain definitive binding epitope information, however it is clear that some parts of the carbohydrate are more important than others for the binding interaction.

Next, we further studied the interaction by computer docking, to determine whether conformational changes occur in the complex.

Docking Studies of GD2 with mAb 3F8

In the absence of a crystal structure for mAb 3F8, a model was generated for the binding of GD2 in the antigen-binding site of

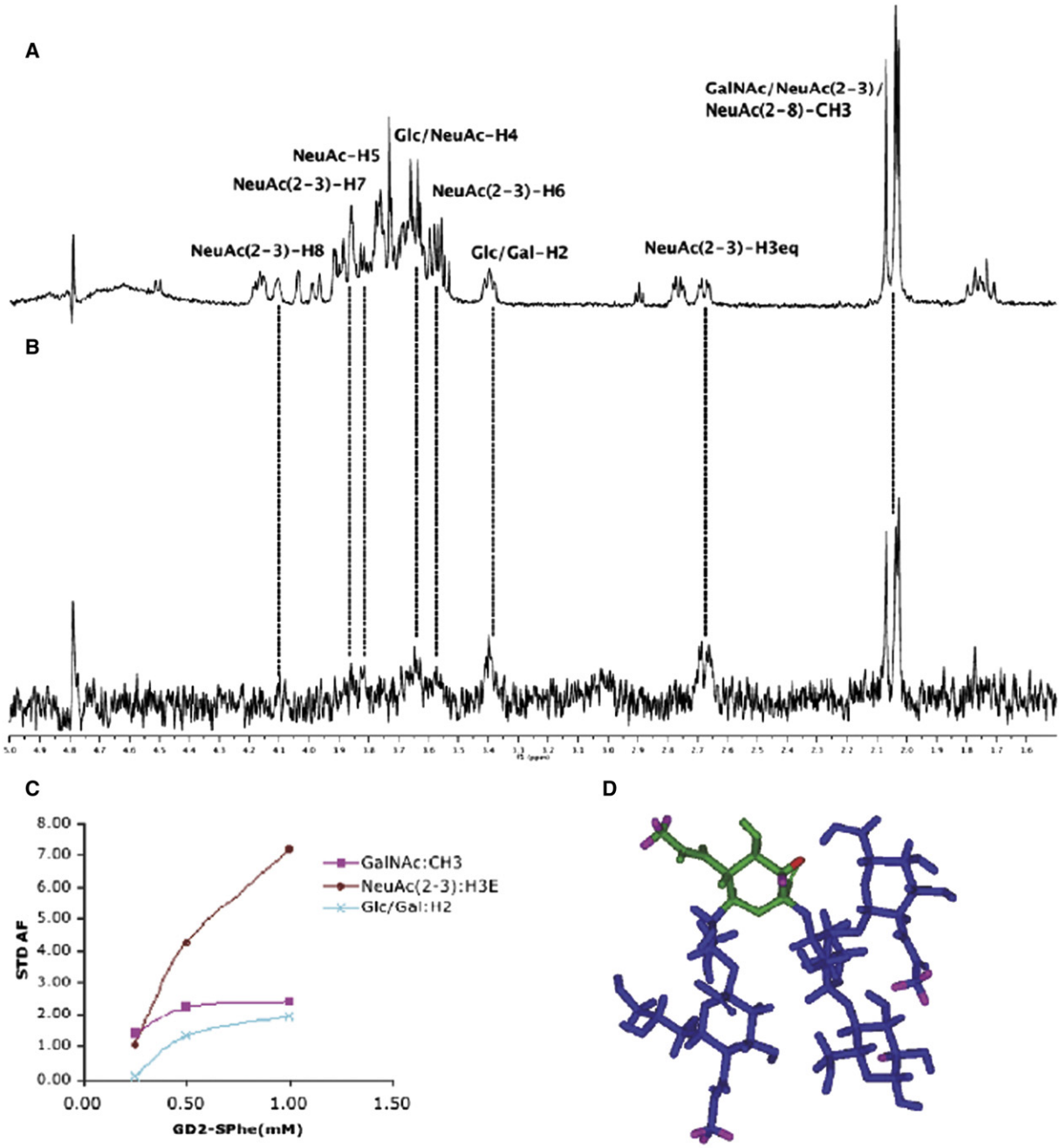

Figure 3. STD NMR Spectra, STD Amplification Factor, and Structure Model of Thiophenyl GD2 Binding to mAb 3F8

(A) Reference spectrum of a mixture of thiophenyl GD2 (500 μM) and 3F8 (10 μM binding sites) at a 50:1 ratio.

(B) STD-NMR spectrum of the same sample (T_{sat} = 5 s).

(C) Observed STD amplification factors of several resonances of thiophenyl GD2 plotted against the ligand concentrations (T_{sat} = 3 s).

(D) The most prominent peaks in the STD spectra arise from the resonances of the residue NeuAc (2-3) in green. Atoms in red correspond to the strongest STD signal, which is assigned a value 100%. Magenta coloring corresponds to residues that are about 20%–40% saturated.

3F8 antibody based on homology modeling with other mAbs. Intermolecular interactions (both electrostatic and hydrophobic) were observed between the GD2 molecule and 3F8 (Figure 4). At the antigen-binding surface, GD2 interacts mainly with residues of light-chain 3 (L3), heavy-chain 2 and 3 (H2 and H3) of complementarity determining region (CDR), as well as with framework residues.

Both the glucose and galactose residues of GD2 bound in the shallow groove in mAb 3F8 between the variable domain light (VL) and variable domain heavy (VH) chains and interact with

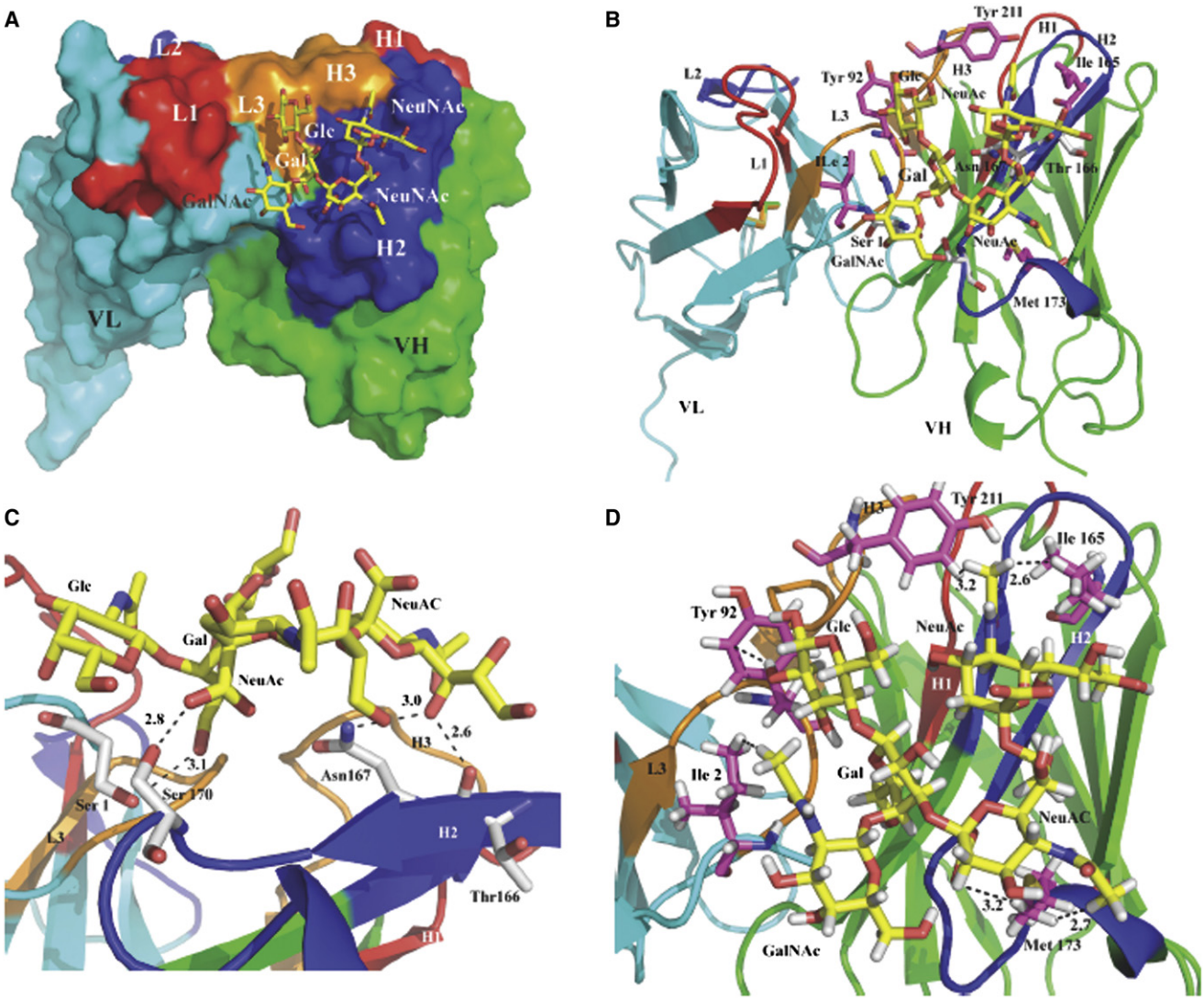

Figure 4. The Predicted Binding Mode of GD2 in the Antigen Binding Surface of a Fab Fragment of 3F8 Antibody

(A) The Fab fragment is displayed as a molecular surface. Color coding is as follows: VL (cyan), VH (green), L1 (red), L2 (blue), L3 (orange), H1 (red), H2 (blue), and H3 (orange). GD2 is depicted as capped sticks with carbon, nitrogen, and oxygen in yellow, blue, and red, respectively.

(B) The Fab of 3F8 VL and VH is displayed as a ribbon structure. Selected residues of 3F8 are represented as thick-capped sticks with carbon, nitrogen, and oxygen in pink, blue, and red, respectively. GD2 is shown as capped sticks, color coded as in (A). Significant nonpolar interactions with GD2 are observed for Ile2 (framework), Tyr 92 (L3), Ile 165, Met 173 (H2), and Tyr 211 (H3). Electrostatic interactions with the GD2 molecule are observed for Ser1 (framework), Thr 166, Asn 167, and Ser170 (H2).

(C) Detailed view of polar interactions between the 3F8 antibody and the GD2 molecule. The Fab of 3F8 VL and VH is displayed as a ribbon structure. Selected residues of 3F8 are represented as thick-capped sticks with carbon, nitrogen, and oxygen in gray, blue, and red, respectively. GD2 is shown as capped sticks, color coded as in (A). Black dashed lines are H-bonds. Distances are measured between the heavy atoms. Ser1 (framework), Thr 166, Asn 167, and Ser170 (H2) form H-bonds with the GD2 molecule.

(D) Hydrophobic interactions between GD2 with the residues of 3F8. These residues are Ile2 (framework), Tyr 92 (L3), Ile 165, Met 173 (H2), and Tyr 211 (H3) are represented as thick-capped sticks with the carbon, nitrogen, oxygen, and hydrogen atoms in pink, blue, red, and white, respectively. Distances are measured between hydrogen atoms.

residues of CDRs. The N-acetylgalactosamine residue occupies the lower part of the groove and the N-acetyl group makes good hydrophobic interactions with framework residue Ile2. Both NeuAcs bind into a relatively flat area of the antigen-binding surface formed mainly by the residues of the H2 CDR and few residues of the H3 CDR (Figures 4A and 4B). Four residues in the antigen binding site hydrogen bond with the GD2 molecule (Figure 4C). The middle NeuAc shows hydrogen-bond interactions with Ser170 on the H2 CDR, whereas the terminal one is largely solvent exposed. The hydroxyl group on the seventh carbon of the terminal NeuAc forms a hydrogen bond with the H2 CDR of 3F8 by way of the backbone carbonyl of Thr166 and the side chain of Asn167. The N-acetyl groups of both Neu5Ac residues make nonpolar contacts with Tyr211, Ile165,

and Met173 (Figure 4D). The calculated binding energy of the 3F8 and GD2 complex was −8.2 kcal/mol (Ki = 0.95 μM).

The bound conformation of GD2 in our docking model is different from the unbound one determined by NMR (rmsd = ~3.0 Å excluding the 2 terminal residues). The GD2/3F8 binding model showed that both NeuNAcs bound into a relatively flat and shallow surface area formed mainly by the residues of H2 CDR loop and a few residues of the H3 CDR loop (Figures 4A and 4B). This may explain why the middle NeuAc (2-3), instead of the terminal one, is the most prominent residue interacting with 3F8 (Figures 3A and 3B).

In order to validate the docking binding model, the theoretical STD effect upon some protons was calculated with the CORCEMA-ST program at different saturation times (Table S4; Experimental Procedures). Taking into account an estimated experimental error of 10%–20% for the STD data, the R-factor (0.42) is indicative of a reasonable fit between the experimental and calculated values. Hence, our binding model is compatible with the experimental STD data.

Together, the STD-NMR epitope mapping of thiophenyl GD2 and ganglioside GD2 with mAb 3F8 and the docking studies of GD2 with 3F8 are consistent, and provide a starting point for designing small molecule ligands of GD2.

Design of Peptidic Ligands

Further support for the predicted region of mAb 3F8 that binds to GD2 comes from the fact that peptide ligands could be designed from this region to mimic the antibody binding surface and yield peptides that interact with GD2 micelles. Small peptidic GD2 ligands M1, M50, and SS58 were designed based on models of the monoclonal antibody 3F8/GD2 complex, mainly mimicking the H2 CDR that curiously also corresponds to a sequence in Tenascin-R (accession number NP_003276), which is reported to be a putative GD2 ligand (Probstmeier et al., 1999). A comparison of anti-GD2 mAbs and TN-R sequences showed high sequence homology between the mAb CDRs and the N-terminal portion of TN-R, which is thought to be the GD2-binding site. It is intriguing that this sequence, ASN-TYR-ASN, is very restricted in the mammalian genome and appears in very few proteins.

Core sequences were flanked by cysteine residues, which, once oxidized, form an intramolecular S-S bond forcing the peptides to adopt the cyclic, β-turn-like conformation seen in CDRs. All peptides were synthesized and tested as control linear analogs devoid of terminal cysteines, to verify the effect of structure on binding. In addition, several control cyclic peptides of related sequences were inactive. To validate the docking binding model and investigate how these peptide ligands bind to GD2, their interactions were studied by NMR and in vitro assays.

Assignments of Peptide Ligand Resonances and Structure Calculations

The sequences and complete proton chemical shift assignments for the 11-residue peptides M50 and SS58 and the 10-residue peptide M1 are provided in Tables S5 and S6. Three-dimensional structures were calculated for M50 and M1 from NMR data. The conformations of these two peptides are relatively flexible in the free state (Table S7). The data show that a random coil is the main secondary structure for M50 (Figure 6) and for M1 (Figure S3), with a β-turn as a minor conformation.

Group Epitope Mapping (GEM): The Binding Interactions of Peptide Ligands M50, M1, and SS58 with GD2 Micelles

The ganglioside GD2 concentration (200 μM) in STD-NMR experiments exceeded the reported critical micelle concentration (CMC) (Sonnino et al., 1994), and 1D-^{1}H NMR spectra showed that it formed micelles in water (data not shown). The STD spectrum indicates that the M50 peptide ligand binds to ganglioside GD2 micelles (Figures 5A and 5B). All of the protons in the M50 peptide experienced some degree of saturation on binding to GD2. Calculation of the STD effects for each resolved proton signal indicated that the tyrosines and Ile4 made the most important contacts with GD2. The aromatic resonances of Tyr1, 6, and 11 could not be resolved to itemize individual effects; however, the overlapping multiplet structure was very similar in the reference and STD spectra, indicating that each aromatic ring contributed equally to the intensity.

STD experiments were recorded at saturation times varying from 1 to 5 s for a 5-fold ligand excess, demonstrating that the maximal amplification factor is reached by 3 s of saturation for residues with weaker interactions such as alanine (Figure 5C). The T1s for the resolved protons in the free peptide were measured using an inversion-recovery pulse sequence, and indicated that at longer relaxation times (>2 s) the STD intensities were dominated by T1 effects. Protons with the longest T1s, such as those in the tyrosine aromatic rings, display the largest STD effect. The initial slope of this plot gives a more accurate reflection of the binding epitope (Yan et al., 2003). Although very short (<1 s) saturation times were not employed in this study, the relevance of tyrosines and isoleucine is indicated from their steeper initial slope in comparison with the resolved glycine or alanine protons. A series of STD titration experiments delivered STD amplifications as a function of ligand excess (Figure 5D). This shows that the maximal effect was not reached under the experimental conditions, which were limited by the necessity to maintain a minimum concentration of GD2 ganglioside to ensure micelle formation.

The interactions of two other peptide ligands (M1 and SS58) with ganglioside GD2 micelles were also investigated by STD experiments (see Figure S4 for STD NMR spectra). STD signals of M1 and SS58 show that the ligands bind to the GD2 micelles. As was observed for M50 (Figure 5), the tyrosines and the methyl resonances of threonine and isoleucine gave the largest STD effects, suggesting that the protein-glycan interactions are dominated by hydrophobic side chains of methyl groups and aromatic rings.

In order to study the conformation of bound ligand, and to complement the STD NMR results, NOESY experiments were recorded for a mixture of M50 and GD2 ganglioside micelles. Many more cross-peaks were observed in the NOESY spectrum of the mixture in comparison to NOESY or ROESY spectra of the free peptide (Figure 6A). For instance, several cross-peaks between Hα and amide (Gly3 -Ala5, Ile4-Asn6, Ile4-Tyr7, Ala5-Tyr7 and Gly9-Try11) were observed. These transferred NOEs showed that the major conformation of the ligand becomes a β-turn ("W" shape) in the bound state as compared with a more flexible β-coil ("U" shape) in the free state (Figures 6B and 6C; Table S7).

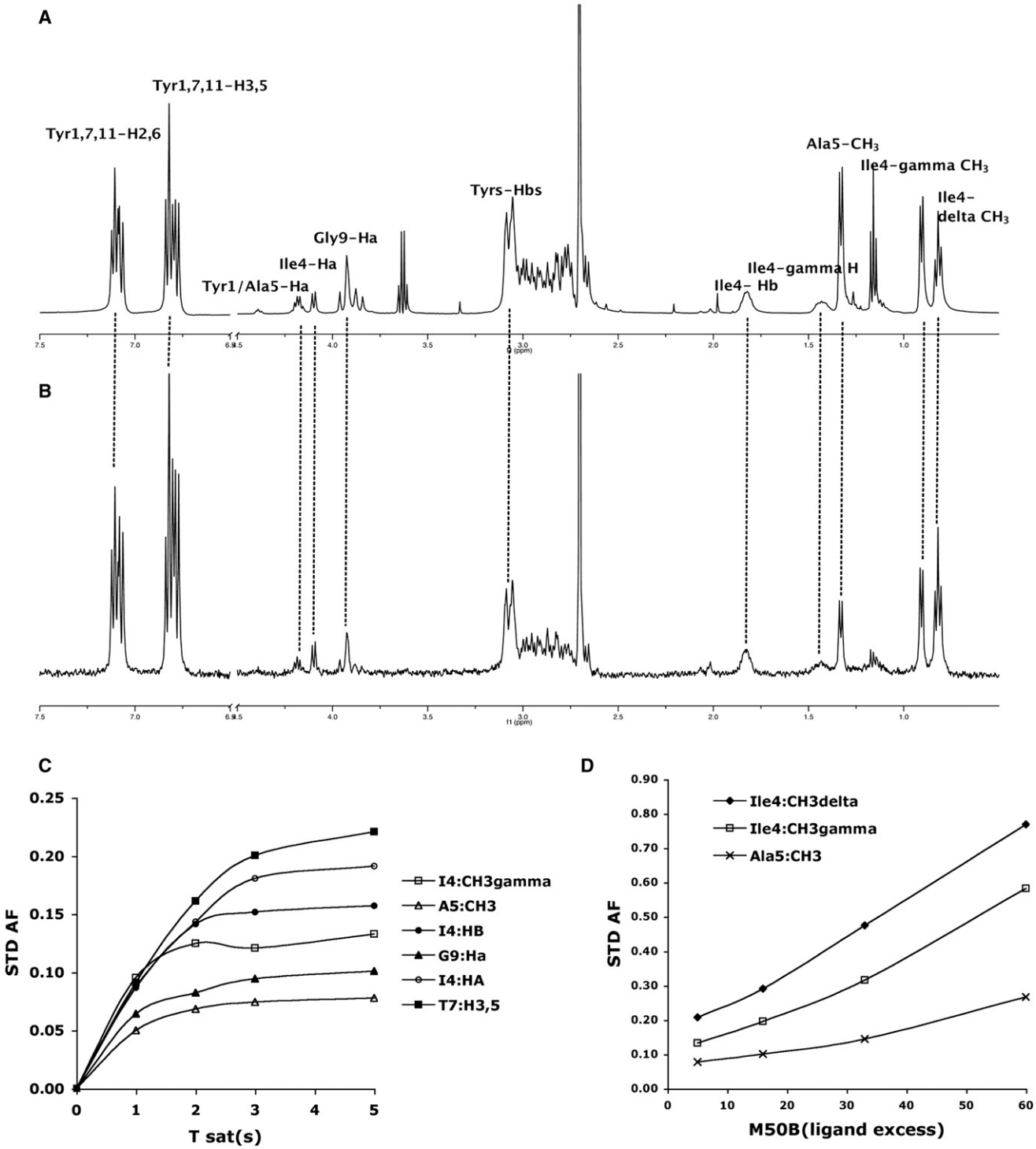

Figure 5. STD-NMR Spectra and STD Amplification Factor for a Mixture of Ganglioside GD2 Micelles and M50B

(A) Reference spectrum of a mixture of ganglioside GD2 micelles (200 μM) and peptide ligand M50B (1 mM) in a ratio of 1:5.

(B) STD-NMR spectrum of the same sample at 298 K (T_{sat} = 5 s).

(C) Observed STD amplification factors of several resonances of peptide ligand M50B plotted against the saturation time in a ratio of 1:5 (ligand excess).

(D) Observed STD amplification factors of several resonances of thiophenyl-GD2 plotted against the ligand concentrations (T_{sat} = 5 s).

Analysis of the average secondary structure of M50 by the software DSSP (Kabsch and Sander 1983) shows that in the bound state there are multiple β-turns with three hydrogen bonds formed, while no hydrogen bonded turns exist in the free state. In the bound state the turns are formed by Cys2 to Ala5, Asn6 to Gly9, and Cys2 to Asn6. In contrast, in the free

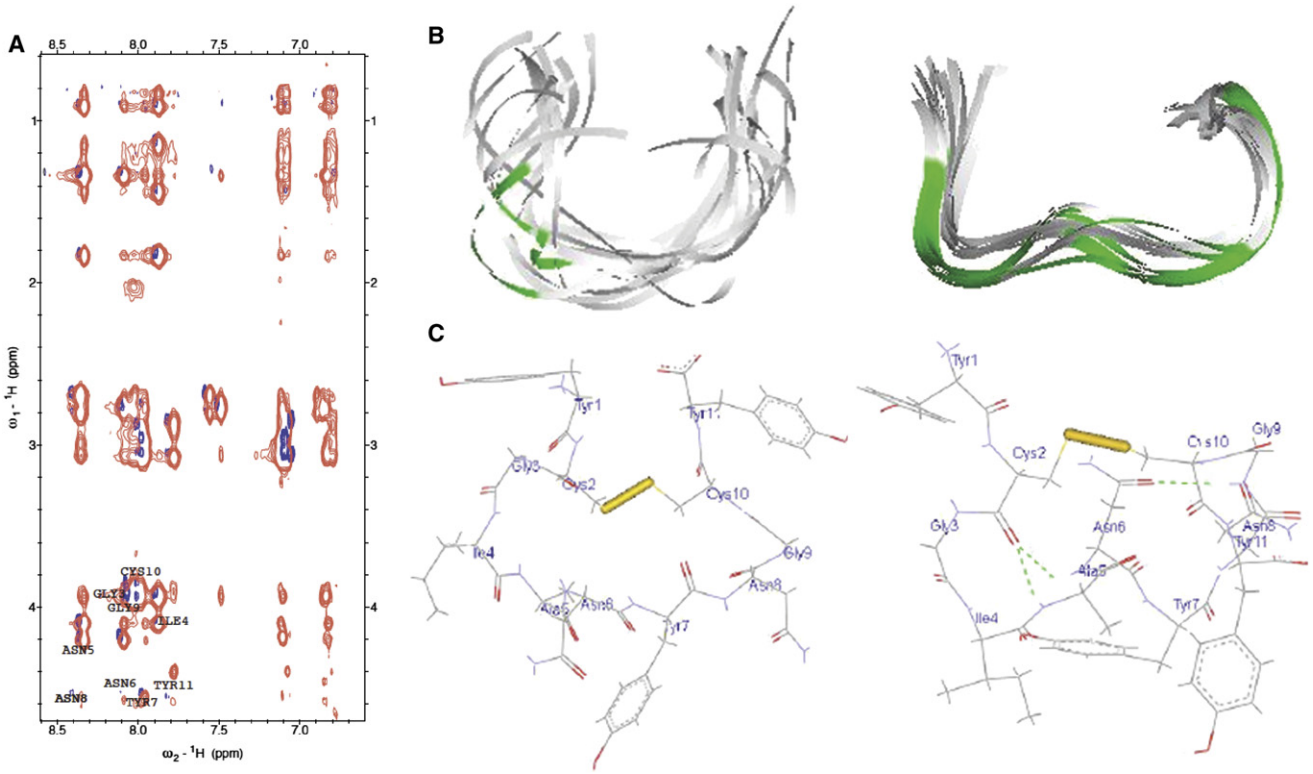

Figure 6. Ensemble of 12 and 19 Lowest-Energy Structures Calculated for the M50B in the Free and Bound State in Water, Respectively

(A) Overlay of ROESY spectrum (black) of M50B in the free state and trans-NOESY spectrum (red) of M50B in the bound state. The mixing times used to record these spectra are 200 and 100 ms, respectively.

(B) The ensembles of structures are in flat ribbon representation and the β turn is in green.

(C) The average structure is in line representation (water molecules are removed). The disulfide bond is in yellow. Three hydrogen bonds between carbonyl group and amide of Cys2 and Ala5, Cys2 and Asn6, and Asn6 and Gly9 are in green.

state the sequence Gly3 to Asn8 forms a more flexible U-shaped β-coil (Figure 6B). The rmsd between these different states is 2.7 Å (calculated for residues 2 to 10).

It appears that the STD spectra were influenced by T1 effects at the longer saturation times used in this study; however, the trNOE results for the peptide show that it adopts a conformation in the presence of GD2 where aromatic and Ile residue side chains are on the same face of the molecule, directed toward the carbohydrate. Although transferred NOE data were not obtained for the other peptidic ligands M1 and SS58, we anticipate that they might also form a similar β-turn upon binding to GD2 because of their high degree of sequence homology to M50.

Together, these data suggest an induced-fit model in which cyclic peptidic ligands adopt a new β-turn conformation upon interacting with GD2. Such β-turn conformation resembles those adopted by antibody CDRs (Saragovi et al., 1992).

Assessment of Ligand Interactions with Gangliosides by Competitive ELISA

The binding specificity of M50, M1, and SS58 was evaluated by competitive ELISA using immobilized gangliosides GD2, GD3, or GM1.

M1 inhibits the binding of mAb 3F8 to GD2 in a dose-dependent manner, with an IC_{50} between 100 and 200 μM. M50 inhibits binding of mAb 3F8 to GD2 by 66% at 200 μM (Figure 7A).

SS58 inhibits the binding of mAb 3F8 to GD2 by 50% at 350 μM. In control assays, SS58 does not prevent cholera toxin B from binding GM1. The peptide also shows weak inhibition of anti-GD3 antibody binding to GD3 (Figure 7B). Thus, the SS58 peptide has excellent selectivity for GD2 over GM1, and good selectivity for GD2 over GD3.

It is possible that SS58 binds to both GD2 and GD3. Whether or not SS58 binds specifically to GD3 is a difficult issue to resolve because the peptide has lower affinity and lower avidity than 3F8. Also, the peptide represents only a selected part of the pharmacophore of 3F8 and some of the 3F8 specificity may have been compromised. GD2 and GD3 have very similar chemical structures, the only difference being that GD2 has an N-acetyl-galactose connecting to the galactose (Figure S2). For these three reasons, especially the closeness of the epitopes of GD2 and GD3, it is not surprising that the peptide could bind to GD3 with low efficacy in the enzyme-linked immunosorbent assay (ELISA) competition assays.

More than 50 control peptides were tested in parallel, including linear analogs of the active cyclic peptides, and several inactive cyclic peptides of related sequences. For example, control peptide 57 (a linear and unstructured analog, see Experimental Procedures) did not block GD2-3F8 interactions (data

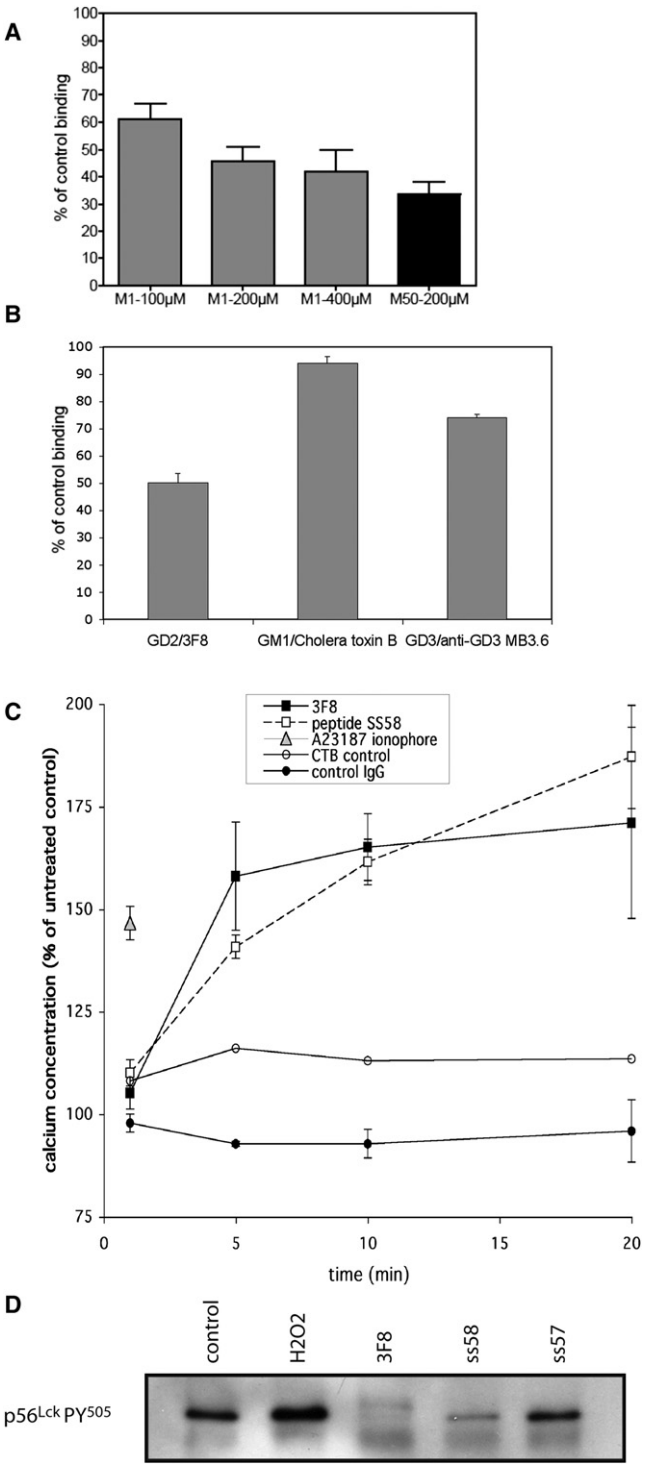

Figure 7. Peptide Ligands M1, M50 and SS58 Selectively Bind to Ganglioside GD2

(A) Binding of peptides M1 and M50 to GD2 was evaluated by their ability to compete anti-GD2 mAb 3F8 binding to immobilized GD2. M1 and M50 strongly inhibit GD2/3F8 interaction. Shown are the averages ± SEM of four to six independent assays, n = 3 per assay.

(B) The selective binding of peptide SS58 to GD2 ganglioside was evaluated by its ability to compete anti-GD2 mAb 3F8, but not anti-GD3 mAb MB3.6 binding to immobilized GD3, or cholera toxin B binding to immobilized GM1. Shown are averages ± SEM of two independent assays, n = 4 per assay.

(C) Peptide SS58 increases intracellular calcium. Live EL4 cells (expressing GD2 and GM1) were treated with mAb 3F8 (13 nM), control mouse IgG (mIg), peptide SS58 (20 μM), the GM1 ligand CTB, or the calcium ionophore A23187; and intracellular calcium concentrations were evaluated over time by flow cytometry using the calcium-sensitive fluorophore Rhod-2 AM. Shown are averages of four independent assays ± SEM.

(D) EL4 cells were treated with control mIgG (13 nM, lane 1), hydrogen peroxide (H_2O_2, 20 mM, lane 2), anti-GD2 mAb 3F8 (13 nM, lane 3), or peptides SS58 (3.3 μM, lane 4) or peptide SS57 (3.3 μM, lane 5) for 20 min at 37°C. The $p56^{Lck}$ immunoprecipitated samples were probed for Tyr^{505} $p56^{Lck}$ using a specific anti-pY^{505} antibody. The blot shown is representative of four independent experiments.

not shown), suggesting that a constraint to induce a β-turn is required; and cyclic peptide NB1.HC1.7 (YCTNYGVCY) derived from a different domain of 3F8 did not inhibit the binding in the ELISA.

Overall the data are consistent with the binding detected by NMR, and with the interpretation that the peptide ligands bind the carbohydrate of GD2.

Functional Mimicry of mAb 3F8

Binding of ganglioside ligands (such as antibodies) to cell surface gangliosides induces Ca^{2+} fluxes (Gouy et al., 1994; Golard, 1998) measurable by the calcium-sensitive fluorophore Rhod-2 AM. The Ca^{2+} fluxes involve the activation of the src family kinases (Hakomori and Zhang, 1997; Golard, 1998; Birkle et al., 2003).

We studied intracellular Ca^{2+} levels and activation of the src family kinase $p56^{LCK}$ in the EL4 thymoma cell line, which expresses GD2 and GM1, but does not express GD3 on the plasma membrane. Exposure of EL4 cells to positive control mAb 3F8 (13 nM) increased intracellular Ca^{2+}. Negative controls (untreated cells or cells treated with nonbinding mouse IgG) do not affect Ca^{2+} levels, and the positive control ionophore increases intracellular Ca^{2+} levels rapidly. This is consistent with the literature (Golard, 1998). Test treatment with SS58 (20 μM) strongly increases the intracellular Ca^{2+}, although the effect is slower than that of mAb 3F8 (Figure 7C). The increased intracellular Ca^{2+} caused by both mAb 3F8 and SS58 can be blocked by the src inhibitor PP1 (data not shown).

In biochemical assays, exposure of EL4 cells to positive control mAb 3F8 or to test SS58 peptide reduced the phosphorylated state of $p56^{LCK}$-$pTyr^{505}$. The negative control linear analog SS57 does not induce $p56^{LCK}$-$pTyr^{505}$ de-phosphorylation, whereas the positive control phosphatase inhibitor H_2O_2 increases the phosphorylated state of $p56^{LCK}$-$pTyr^{505}$ (Figure 7D). These results are consistent with the above studies of Ca^{2+} fluxes. The $p56^{LCK}$-$pTyr^{505}$ is an inhibitory phosphotyrosine, and its dephosphorylation is required for activation of the kinase enzymatic activity of $p56^{LCK}$, leading to Ca^{2+} fluxes (Palacios and Weiss, 2004). In further control assays, treatment of a GD2-negative subclone of EL4 cells with peptide SS58 did not activate $p56^{Lck}$, even though these cells express the same levels of $p56^{Lck}$ as the parental GD2 cells (data not shown).

Together the data show that functionally these small peptidic ligands of GD2 activate signaling pathways in live cells in a manner similar to mAb 3F8.

SIGNIFICANCE

In this study, the combined use of STD-NMR spectroscopy, transferred NOE experiments, and molecular modeling furnished details on the molecular recognition of the ganglioside GD2 by the monoclonal antibody 3F8; specifically, it furnished details of conformational changes in the antibody CDR loops. Moreover, similar NMR experiments were performed on complexes between GD2 and three small peptide ligands, which were designed using the structural information and which were validated in binding and functional studies.

The present work reveals the key pharmacophoric groups that are required for the recognition of the cell-surface carbohydrate epitope recognized by the mAb 3F8 and suggests an induced-fit mechanism through which unstructured antibody CDRs may adopt a β-turn conformation upon interacting with GD2.

Our work furthers the concept that it is possible to develop small-molecule ligands of highly flexible targets such as ganglioside carbohydrates, and rationalizes that gangliosides may be druggable targets. The structural information gleaned from studying the protein- and peptide-carbohydrate interactions has enhanced understanding of ganglioside-ligand interactions and may facilitate design of improved GD2 ligands, and ligands for other gangliosides.

EXPERIMENTAL PROCEDURES

Synthesis of Thiophenyl GD2

Thiophenyl GD3 was synthesized from thiophenyl Lac as described previously (Houliston et al., 2007). Thiophenyl GD2 (Figure 1A) was synthesized from thiophenyl GD3 using a recombinant β-1,4-*N*-acetylgalactosaminyltransferase (CgtA, construct CJL-30) and an UDP-GlcNAc 4-epimerase (Gne, construct CPG-13) originally cloned from *Campylobacter jejuni* (Bernatchez et al., 2005; Blixt et al., 2005). The sample was purified (>98%) by high-performance liquid chromatography (HPLC) (Waters 600) using a C-18 semipreparative column (Phenomenex), and was verified by electrospray ionization mass spectrometry and NMR. The measured molecular weight of thiophenyl GD2 corresponded to expected values.

Peptide Ligand Synthesis

Peptides were designed based on the structures of mAb 3F8 and Tenascin-R. Peptide ss58 is YCGGIANYNCY, peptide M1 is YCGTNYNGCY, and peptide M50 is YCGIANYNGCY. Peptide SS57 is a linear analog that can not cyclize, with sequence GGIANYNTS. Peptides were synthesized with an Advanced Chemtech automatic synthesizer using solid-phase Fmoc chemistry. After cleavage from resin and side-chain deprotection, peptides were subjected to cyclization by oxidation (which caused disulfide-bond formation) at 4°C under O_2 in 50 mM ammonium bicarbonate (pH 8.5). Cyclic peptides were repurified (>95%) by HPLC (Varian) using a C-18 preparative column (Phenomenex), and were characterized by mass spectrometry and NMR spectroscopy. The measured molecular weight of linear and cyclic peptides corresponded to expected values.

Quantification of Thiophenyl GD2–3F8 mAb Interactions by Competitive ELISA

Gangliosides GD2 or GD3 (Advanced ImmunoChemical Inc.) (10 ng/well, in ethanol) were immobilized onto polystyrene Corning Strip Well 96-well plates (Fisher Scientific) by evaporation in a fume hood for 2 hr. The wells were then filled with phosphate-buffered saline containing 0.5% bovine serum albumin (PBS-0.5% BSA) for 1 hr. In competition assays, increasing concentrations of soluble ganglioside, dissolved in PBS, were added to the plates for 30 min before adding the mAbs. Then, anti-GD2 monoclonal antibody 3F8 (5 ng/well) (prepared and characterized in house [Cheung et al., 1985]) or anti-GD3 monoclonal antibody R24 (15 ng/well) (Abcam) was added for 15 min. The plates were washed three times with PBS-0.5% BSA and incubated 20 min with 1/1000 dilution of horseradish peroxidase-conjugated anti-mouse antibody (Sigma). After three washes with PBS-0.5% BSA and two with PBS, the colorimetric substrate TMB One Solution (Promega) was added, and the reaction stopped with 0.5 N H_2SO_4 and the plates were read at 450 nm (Benchmark Plus, Bio-Rad). Wells with no mAb added were treated as background and standardized as 0% binding. Wells with no competitor ganglioside added were standardized as 100% binding.

NMR Spectroscopy

All NMR experiments were carried out on a 500 MHz Varian INOVA NMR spectrometer equipped with a triple-resonance H {CN} cold probe and z-axis pulsed field gradients. 2D NMR spectra were processed by NMRPipe (Delaglio et al., 1995) and assigned by SPARKY 3 (T. D. Goddard and D. G. Kneller, University of California, San Francisco).

NMR Spectroscopy of Ganglioside GD2 and Thiophenyl GD2

Mixed micelles were prepared by dissolving ganglioside GD2 (1 mM) and the detergent dodecylphosphocholine-d38 (DPC, molar ratio 1:40) in deuterated 50 mM phosphate buffer (pD 6.6) (Acquotti et al., 1990). Thiophenyl GD2 was dissolved in deuterated 50 mM phosphate buffer. Spectra were obtained at 308 K or 298 K, respectively. ^{1}H-^{1}H gradient-selected COSY spectra, DQF-COSY, TOCSY, ROESY with 200 ms, NOESY spectra with mixing times of 50–200 ms, ^{13}C HMBC, and HSQC spectra were recorded. ^{1}H chemical shifts were referred to an internal sodium 2,2-dimethyl-2-silapentane-5-sulfonate standard at 0.00 ppm. ^{13}C chemical shifts were indirectly referenced to the proton frequency (see additional details in the Supplemental Experimental Procedures).

NMR Spectroscopy of Peptide Ligands

Samples contained M1, M50, or SS58 in 10% D_2O/90% H_2O (v/v) or 100% D_2O at pH 6.0 or 3.0, at 298 K. Standard experimental protocols were used for TOCSY, phase-sensitive double quantum filtered-COSY, COSY-30, NOESY, and ROESY spectra.

STD-NMR Spectroscopy

A 1D saturation transfer difference pulse sequence with internal subtraction via phase cycling was employed to record difference spectra (Mayer and Meyer, 2001). On-resonance irradiation of GD2 gangliosides and mAb 3F8 was performed at 0 ppm, except in the case of GD2-DPC micelles, where on resonance irradiation of the antibody was at −2 ppm. Off-resonance irradiation was at 34.8 ppm. Reference spectra were recorded using the same pulse sequence with saturation pulses applied at 34.8 ppm, and no internal subtraction. Experiments were recorded with saturation times of 5 s, 3 s, 2 s, and 1 s. Spectra were recorded with 32000 points, a sweep width of 16 ppm, and 1024 to 2048 transients (see additional details in the Supplemental Experimental Procedures). STD spectra were processed by MestReNova-Lite v5.2.1-3586 (Mestrelab Research SL). To test the shaped pulse selectivity, STD experiments on thiophenyl-GD2, M50B, M1, and GD2 in DPC micelles alone without antibody were acquired. No ligand signals were present in the STD spectra for thiophenyl-GD2, M50B, and M1. However, there is a nonspecific signal of methyl groups for GD2 in DPC micelles. Inversion-recovery experiments to measure longitudinal relaxation times (T1) for free thiophenyl-GD2 and M50 were acquired. For the titration and saturation experiments, we used the STD amplification factor (Mayer and Meyer, 2001) for a better assessment of the absolute magnitude of the STD effect. After the STD-NMR experiments, transient transferred NOE experiments employing different mixing times were performed.

Sample Preparation for Thiophenyl GD2 and mAb 3F8/Ganglioside GD2 in DPC and mAb 3F8 Interactions

3F8 was concentrated using Amicon centrifugal filters (10 kDa cutoff, Millipore) and exchanged several times with a deuterated 50 mM phosphate buffer (pH 6.0). The mAb preparations were combined with freeze-dried thiophenyl GD2 or ganglioside GD2 in DPC (CDN Isotopes) micelles at molar ratios ranging from 1:25 to 1:200; the final oligosaccharide concentrations were

between 0.125 and 1 mM. Difference spectra were recorded for ligand in the absence of binding partner to confirm that the ligand was not excited by the saturation pulses at 0 ppm.

Sample Preparation for Peptide Ligands Bound to Ganglioside GD2 Micelles

The ganglioside GD2 was subjected to three cycles of freeze-drying with D_2O to remove traces of water and to prepare a stock solution with a final concentration of 3 mM in deuterated 50 mM phosphate buffer (pH 6.2). Dilution effects from addition of this GD2 stock solution to peptide ligands solution to make different ratios were minimal. Stock solutions of peptide ligands, 2 to 3 mM each, were prepared by dissolving them in deuterated 50 mM phosphate buffer. The concentrations of the peptides were determined by UV (Nanodrop 1000, Wilmington) at 280 nM. 1D STD-NMR spectra were acquired at 298 K for a variety of peptide to GD2 ratios.

Structure Calculations

Different mixing times of NOESY spectra were used to evaluate the linear build-up of NOEs. Molecular dynamics simulations with NMR refinement in the AMBER 9 GB Model (Case et al., 2005) with the force field (Glycam_04.dat [Woods et al., 1995] and GAFF [Wang et al., 2004]) were employed to determine the energetically favorable conformations of the two types of unbound ganglioside. The topology file of truncated ceramide was produced by ANTECHAMBER (Wang et al., 2006). 3D structures of peptide ligands were calculated by the software ARIA 2.2/CNS 1.2 with the network anchoring approach (Rieping et al., 2007). From the 200 structures calculated for each peptide, the 20 lowest energy ones were chosen and clustered by MMTSB (Feig et al., 2004). Structures were visualized using Discovery Studio 1.7 (Accelrys), PyMOL, and VMD-Xplor on Mac OS X (see additional details in the Supplemental Experimental Procedures).

Docking Studies

Structure Prediction, Model Building, and Refinement

The crystal structure of malaria antigen AMA1 antibody Fab (Protein Data Bank [PDB] code 2q8a) (Coley et al., 2006) and 13G5 antibody Fab (PDB code 2gjz) (Muller et al., 2007) were selected as templates for the light chain (84%) and heavy chain (84%) of 3F8, respectively. The homology modeling was carried out using the program COMPOSER in SYBYL 7.3 (Tripos). Structural refinement of the complex was done by stepwise energy minimization in Sybyl using the AMBER all-atom force field to a gradient of 0.05 kcal/mol/Å. This energy-minimized model was then used as starting point for MD simulation in explicit water, using the AMBER ff03 force field in the AMBER 9. The MD average structure was obtained from the most stable part of the trajectory for docking study (see additional details in Supplemental Experimental Procedures and Figures S5 and S6).

Molecular Docking of GD2 and CORCEMA-ST Calculations

The GD2 docking in the putative binding site of Fab fragment of 3F8 was performed with in-house docking software (S.C. and E.O.P., unpublished data). A box around the 6 CDRs of the heavy and light chain of 3F8 was constructed and defined the binding region to be searched. In order to sample various conformations, 12,000 conformers of GD2 were generated from snapshots taken from an MD simulation (12 ns) in explicit water using AMBER ff03 and GAFF force fields starting from the NMR structures. Partial charges of the conformers were calculated by the AM1-BCC method (Jakalian et al., 2002). Each of the docked conformers of GD2 was exhaustively docked into the 3F8 Fab and scored. The top-scoring 100 poses were clustered. The most populated cluster was taken to be representative of the true GD2 binding mode in the Fab of 3F8 antibody. The best-scored pose from this cluster was selected to represent the binding model. This pose was subjected to minimization followed by a 5 ns MD simulation. The MD trajectory was used to calculate a predicted binding free energy of the complex using a solvated interaction energy (SIE) approach (Naim et al., 2007). Then, CORCEMA-ST (Jayalakshmi and Krishna, 2002) program was used to calculate theoretical STD effects (see additional details in Supplemental Experimental Procedures).

Detection of Peptide-Ganglioside Interaction by Competitive ELISA

ELISAs were as described above, except that cyclic or linear peptides (50 μg/well, in PBS) were added to the wells as putative competitors for 1 hr before anti-ganglioside antibodies or anti-GM1 cholera toxin-B (CTB). Selectivity of competitive inhibition of GD2-3F8 interactions was determined by monitoring the effect upon GM1-CTB and GD3-anti-GD3 interactions. Wells with no peptide added or control irrelevant peptide added were standardized as 100% binding. Wells with no 3F8 added and also wells where 3F8 was replaced with mouse IgG were standardized as 0% binding.

Intracellular Calcium Studies

GD2-expressing EL4 thymoma cells (1×10^6 per sample) were washed with Ringer's solution (155 mM NaCl, 4.5 mM KCl, 2 mM $CaCl_2$, 1 mM $MgCl_2$, 10 mM D-glucose, 5 mM HEPES) and resuspended in 1 ml Ringer's for 15 min at 37°C. Then 5 μM Rhod-2AM (Molecular Probes) was added to the cells and incubated for 30 min at room temperature with mild agitation. Cells were washed, and resuspended in 1 ml Ringer's, and incubated for 30 min, after which cells were stimulated with the indicated ganglioside ligands (or calcium ionophore A23187 as control) and analyzed over a 30 min period for intracellular Ca^{2+} using a flow cytometer (Becton Dickinson).

Ex Vivo T Cell Receptor Activation

EL4 thymoma cells (5×10^6 per sample) in culture media were treated with control mouse IgG (13 nM), mAb 3F8 (13 nM), peptides 57 and 58 (3.3 μM), or hydrogen peroxide (20 mM) for 20 min at 37°C. After lysis in mild lysis buffer (10 mM CHAPS, 0.15 M NaCl, 0.01 M sodium phosphate [pH 7.2], 2 mM EDTA, 50 mM sodium fluoride, EDTA-free protease inhibitor cocktail [Roche]), p56Lck protein was immunoprecipitated with protein A-agarose beads (Upstate Biotechnology) coated with anti-$p56^{Lck}$ mAb 3A5 (Santa Cruz) and samples were probed in western blots for Tyr505 $p56^{Lck}$ using rabbit anti-PY505 antibody (Abcam).

SUPPLEMENTAL INFORMATION

Supplemental Information includes seven figures, seven tables, Supplemental Experimental Procedures, and Supplemental References and can be found with this article online at doi:10.1016/j.chembiol.2010.01.012.

ACKNOWLEDGMENTS

Supported by the Canadian Institutes of Health Research (MOP77577 to WDL; MOP192060 to HUS; and MOP-81277 to KG). NMR experiments were recorded at the Québec/Eastern Canada High Field NMR Facility, supported by grants from the Canada Foundation for Innovation, the Natural Sciences and Engineering Research Council of Canada, and the Fonds de la Recherché en Santé du Québec (FRSQ). W.Y.T. received a scholarship from the FRSQ, and from the Montreal Center for Experimental Therapeutics in Cancer. We thank Warren Wakarchouk (IBS-NRCC) and Marie-France Karwaski (IBS-NRCC) for the synthesis of thiophenyl-GD3 and thiophenyl-GD2, and Teresa Lama (Mimetogen Pharmaceuticals) for peptide synthesis.

Received: August 11, 2009
Revised: December 18, 2009
Accepted: January 26, 2010
Published: February 25, 2010

REFERENCES

Acquotti, D., Poppe, L., Dabrowski, J., Von der Lieth, C., Sonnino, S., and Tettamanti, G. (1990). Three-dimensional structure of the oligosaccharide chain of GM1 ganglioside revealed by a distance-mapping procedure: a rotating and laboratory frame nuclear overhauser enhancement investigation of native glycolipid in dimethyl sulfoxide and in water-odecylphosphocholine solutions. J. Am. Chem. Soc. *112*, 7772–7778.

Bernatchez, S., Szymanski, C.M., Ishiyama, N., Li, J., Jarrell, H.C., Lau, P.C., Berghuis, A.M., Young, N.M., and Wakarchuk, W.W. (2005). A single bifunctional UDP-GlcNAc/Glc 4-epimerase supports the synthesis of three cell surface glycoconjugates in Campylobacter jejuni. J. Biol. Chem. *280*, 4792–4802.

Birkle, S., Zeng, G., Gao, L., Yu, R.K., and Aubry, J. (2003). Role of tumor-associated gangliosides in cancer progression. Biochimie *85*, 455–463.

Blixt, O., Vasiliu, D., Allin, K., Jacobsen, N., Warnock, D., Razi, N., Paulson, J.C., Bernatchez, S., Gilbert, M., Wakarchuk, W., et al. (2005). Chemoenzymatic synthesis of 2-azidoethyl-ganglio-oligosaccharides GD3, GT3, GM2, GD2, GT2, GM1, and GD1a. Carbohydr. Res. *340*, 1963–1972.

Cahan, L.D., Irie, R.F., Singh, R., Cassidenti, A., and Paulson, J.C. (1982). Identification of a human neuroectodermal tumor antigen (OFA-I-2) as ganglioside GD2. Proc. Natl. Acad. Sci. USA *79*, 7629–7633.

Case, D.A., Cheatham, T.E., 3rd, Darden, T., Gohlke, H., Luo, R., Merz, K.M., Jr., Onufriev, A., Simmerling, C., Wang, B., Woods, R.J., et al. (2005). The Amber biomolecular simulation programs. J. Comput. Chem. *26*, 1668–1688.

Chatterjee, C., and Mukhopadhyay, C. (2005). Interaction and structural study of kinin peptide bradykinin and ganglioside monosialylated 1 micelle. Biopolymers *78*, 197–205.

Chatterjee, C., Majumder, B., and Mukhopadhyay, C. (2004). Pulsed-field gradient and saturation transfer difference NMR study of enkephalins in the ganglioside GM1 micelle. J. Phys. Chem. B *108*, 7430–7436.

Cheresh, D.A., Rosenberg, J., Mujoo, K., Hirschowitz, L., and Reisfeld, R.A. (1986). Biosynthesis and expression of the disialoganglioside GD2, a relevant target antigen on small cell lung carcinoma for monoclonal antibody-mediated cytolysis. Cancer Res. *46*, 5112–5118.

Cheung, N.-K.V., Saarinen, U.M., Neely, J.E., Landmeier, B., Donovan, D., and Coccia, P.F. (1985). Monoclonal antibodies to a glycolipid antigen on human neuroblastoma cells. Cancer Res. *45*, 2642–2649.

Coley, A.M., Parisi, K., Masciantonio, R., Hoeck, J., Casey, J.L., Murphy, V.J., Harris, K.S., Batchelor, A.H., Anders, R.F., and Foley, M. (2006). The most polymorphic residue on Plasmodium falciparum apical membrane antigen 1 determines binding of an invasion-inhibitory antibody. Infect. Immun. *74*, 2628–2636.

Delaglio, F., Grzesiek, S., Vuister, G.W., Zhu, G., Pfeifer, J., and Bax, A. (1995). NMRpipe: a multidimensional spectral processing system based on UNIX pipes. J. Biomol. NMR *6*, 277–293.

Dube, D.H., and Bertozzi, C.R. (2005). Glycans in cancer and inflammation–potential for therapeutics and diagnostics. Nat. Rev. Drug Discov. *4*, 477–488.

Feig, M., Karanicolas, J., and Brooks, C.L. (2004). MMTSB Tool Set: enhanced sampling and multiscale modeling methods for applications in structural biology. J. Mol. Graph. Model. *22*, 377–395.

Golard, A. (1998). Anti-GM3 antibodies activate calcium inflow and inhibit platelet- derived growth factor beta receptors (PDGFbetar) in T51B rat liver epithelial cells. Glycobiology *8*, 1221–1225.

Gouy, H., Deterre, P., Debre, P., and Bismuth, G. (1994). Cell calcium signaling via GM1 cell surface gangliosides in the human Jurkat T cell line. J. Immunol. *152*, 3271–3281.

Hakomori, S., and Zhang, Y. (1997). Glycosphingolipid antigens and cancer therapy. Chem. Biol. *4*, 97–104.

Houliston, R.S., Yuki, N., Hirama, T., Khieu, N.H., Brisson, J.-R., Gilbert, M., and Jarrell, H.C. (2007). Recognition characteristics of monoclonal antibodies that are cross-reactive with gangliosides and lipooligosaccharide from Campylobacter jejuni strains associated with Guillain-Barre and Fisher syndromes. Biochemistry *46*, 36–44.

Jakalian, A., Jack, D.B., and Bayly, C.I. (2002). Fast, efficient generation of high-quality atomic charges. AM1-BCC model: II. Parameterization and validation. J. Comput. Chem. *23*, 1623–1641.

Jayalakshmi, V., and Krishna, N.R. (2002). Complete relaxation and conformational exchange matrix (CORCEMA) analysis of intermolecular saturation transfer effects in reversibly forming ligand-receptor complexes. J. Magn. Reson. *155*, 106–118.

Ji, Z., Yao, Z., and Liu, M. (2009). Saturation transfer difference nuclear magnetic resonance study on the specific binding of ligand to protein. Anal. Biochem. *385*, 380–382.

Kabsch, W., and Sander, C. (1983). Dictionary of protein secondary structure: pattern recognition of hydrogen-bonded and geometrical features. Biopolymers *22*, 2577–2637.

Mandal, P.K., and Pettegrew, J.W. (2004). Alzheimer's disease: NMR studies of asialo (GM1) and trisialo (GT1b) ganglioside interactions with Abeta(1-40) peptide in a membrane mimic environment. Neurochem. Res. *29*, 447–453.

Mayer, M., and Meyer, B. (2001). Group epitope mapping by saturation transfer difference nmr to identify segments of a ligand in direct contact with a protein receptor. J. Am. Chem. Soc. *123*, 6108–6117.

Meyer, B., and Peters, T. (2003). NMR spectroscopy techniques for screening and identifying ligand binding to protein receptors. Angew. Chem. Int. Ed. Engl. *42*, 864–890.

Modak, S., and Cheung, N.K. (2007). Disialoganglioside directed immunotherapy of neuroblastoma. Cancer Invest. *25*, 67–77.

Muller, R., Debler, E.W., Steinmann, M., Seebeck, F.P., Wilson, I.A., and Hilvert, D. (2007). Bifunctional catalysis of proton transfer at an antibody active site. J. Am. Chem. Soc. *129*, 460–461.

Naim, M., Bhat, S., Rankin, K.N., Dennis, S., Chowdhury, S.F., Siddiqi, I., Drabik, P., Sulea, T., Bayly, C.I., Jakalian, A., et al. (2007). Solvated interaction energy (SIE) for scoring protein-ligand binding affinities. 1. Exploring the parameter space. J. Chem. Inf. Model. *47*, 122–133.

Palacios, E.H., and Weiss, A. (2004). Function of the Src-family kinases, Lck and Fyn, in T-cell development and activation. Oncogene *23*, 7990–8000.

Probstmeier, R., Michels, M., Franz, T., Chan, B.M.C., and Pesheva, P. (1999). Tenascin-R interferes with integrin-dependent oligodendrocyte precursor cell adhesion by a ganglioside-mediated signalling mechanism. Eur. J. Neurosci. *11*, 2474–2488.

Rieping, W., Habeck, M., Bardiaux, B., Bernard, A., Malliavin, T.E., and Nilges, M. (2007). ARIA2: Automated NOE assignment and data integration in NMR structure calculation. Bioinformatics *23*, 381–382.

Saragovi, H.U., Greene, M.I., Chrusciel, R.A., and Kahn, M. (1992). Loops and secondary structure mimetics: development and applications in basic science and rational drug design. Biotechnology (N. Y.) *10*, 773–778.

Sonnino, S., Cantù, L., Corti, M., Acquotti, D., and Venerando, B. (1994). Aggregative properties of gangliosides in solution. Chem. Phys. Lipids *71*, 21–45.

Svennerholm, L., Bostrom, K., Jungbjer, B., and Olsson, L. (1994). Membrane lipids of adult human brain: lipid composition of frontal and temporal lobe in subjects of age 20 to 100 years. J. Neurochem. *63*, 1802–1811.

Thurin, J., Thurin, M., Herlyn, M., Elder, D.E., Steplewski, Z., Clark, W.H., and Koprowski, H. (1986). GD2 ganglioside biosynthesis is a distinct biochemical event in human melanoma tumor progression. FEBS Lett. *208*, 17–22.

Vasudevan, S.V., and Balaji, P.V. (2001). Dynamics of ganglioside headgroup in lipid environment: Molecular dynamics simulations of GM1 embedded in dodecylphosphocholine micelle. J. Phys. Chem. B *105*, 7033–7041.

Vasudevan, S.V., and Balaji, P.V. (2002). Comparative analysis of ganglioside conformations by MD simulations: implications for specific recognition by proteins. J. Mol. Struct. THEOCHEM *583*, 215–232.

Wang, J., Wolf, R.M., Caldwell, J.W., Kollman, P.A., and Case, D.A. (2004). Development and testing of a general amber force field. J. Comput. Chem. *25*, 1157–1174.

Wang, J., Wang, W., Kollman, P.A., and Case, D.A. (2006). Automatic atom type and bond type perception in molecular mechanical calculations. J. Mol. Graph. Model. *25*, 247–260.

Watanabe, T., Pukel, C.S., Takeyama, H., Lloyd, K.O., Shiku, H., Li, L.T., Travassos, L.R., Oettgen, H.F., and Old, L.J. (1982). Human melanoma antigen AH is an autoantigenic ganglioside related to GD2. J. Exp. Med. *156*, 1884–1889.

Woods, R.J., Dwek, R.A., Edge, C.J., and Fraser-Reid, B. (1995). Molecular mechanical and molecular dynamic simulations of glycoproteins and oligosaccharides. 1. GLYCAM_93 parameter development. J. Phys. Chem. *99*, 3832–3846.

Yan, J., Kline, A.D., Mo, H., Shapiro, M.J., and Zartler, E.R. (2003). The effect of relaxation on the epitope mapping by saturation transfer difference NMR. J. Magn. Reson. *163*, 270–276.

Yuki, N., Yamada, M., Tagawa, Y., Takahashi, H., and Handa, S. (1997). Pathogenesis of the neurotoxicity caused by anti-GD2 antibody therapy. J. Neurol. Sci. *149*, 127–130.